LAWRENCE
LIVERMORE
NATIONAL
LABORATORY

UCRL-CONF-206675

Transferring Electron Beam Welding Parameters Between DIfferent Machines and Facilities Using Advanced Diagnostics

John W. Elmer, Todd A. Palmer, Peter Terrill, K. D. Knicklas, T. M. Mustaleski, Paul Burgardt

September 21, 2004

57th Annual Assembly of the International Institute of Welding
Osaka, Japan
July 11, 2004 through July 16, 2004

Transferring Electron Beam Welding Parameters Between Different Machines and Facilities Using Advanced Diagnostics

J.W. Elmer, T.A. Palmer, P. Terrill, K.D. Nicklas‡, T. Mustaleski‡, and P. Burgardt*

Lawrence Livermore National Laboratory
Livermore, CA, USA

‡BWXT Y-12 Plant
Oak Ridge, TN, USA

*Los Alamos National Laboratory
Los Alamos, NM, USA

Abstract

Transferring electron beam (EB) welding parameters between different welders can be a costly and time consuming process requiring the completion of expensive weld parameter studies. In order to modernize and streamline this process, the LLNL Beam Profiler diagnostic tool, which has been developed and tested at Lawrence Livermore National Laboratory (LLNL) to measure the size, shape, and power density distribution of electron beams, is currently being used to characterize the performance of EB machines at several U.S. Department of Energy facilities. The characterization of these machines involves performing defocus studies on each welder to measure the properties of 1 kW beams made at constant current, voltage, and work distance settings. Using these carefully characterized beams, autogenous welds on 304L stainless steel were then made at LLNL and replicated on the other machines. A key finding from these studies was that the widespread use of work distance values measured from the surface of the part being welded to the top of the EB vacuum chamber are suitable only for machines with a similar upper column design. Otherwise, the focus-lens to part distance must be determined and controlled. A simple method for determining the focus-lens to part distance with the LLNL Beam Profiler diagnostic tool is presented. The ability to transfer EB welds between machines represents a major accomplishment in the development and more widespread use of this diagnostic tool. This work also serves as a basis for the continuing development of procedures and equipment for characterizing electron beams and as a precursor to the development of a modern weld transfer procedure.

Introduction

There are several primary process parameters in electron beam welding, including the beam voltage, current, focus coil current, travel speed, work distance, and vacuum level. The selection of these parameters to produce a weld meeting a given set of design requirements is a subjective process which relies heavily on operator experience and costly and time-consuming parametric studies. Of these beam parameters, the determination of the "sharp focus" condition is the most difficult to define and the most difficult to reproduce on a consistent basis. During this focusing operation, the strength of the magnetic lens is changed, thus arbitrarily raising or lowering the sharp focus position in the weld chamber. The beam is focused by the operator who adjusts the focus coil current settings while observing the light emitted from a high melting point target material, such as tungsten. When the emitted light reaches a maximum intensity, the beam is considered to be at "sharp focus".[1]

The reproducibility of the beams produced at a given focus setting on a given machine is not guaranteed. Different operators may interpret the brightest emission from the target material differently, resulting in different "sharp focus" conditions. An inconsistently focused beam can result in significant variations in the weld width and depth. These difficulties are only compounded when the parameters selected for one machine are transferred to other machines. For example, the focus setting on one machine may not match that of another, due to differences in the focusing lens and the construction of the upper column of the welder. As a result, the current density of each beam can differ, resulting in welds of differing dimensions. With so many unknown or little understood relationships, the transfer of electron beam welding parameters becomes a costly and time-intensive operation.

A quantitative knowledge of the properties of the electron beams produced by these machines is attainable through the use of advanced diagnostic tools [2-8]. Such a tool has been developed at Lawrence Livermore National Laboratory (LLNL) over the past decade in an attempt to quantify the properties of electron beams used for welding.[5-8] This system collects the beam through a series of radial slits as the beam is oscillated in the shape of a circle over a tungsten disk. Once the data from the beam is collected, computer tomography algorithms are used to reconstruct the power density distribution of the beam. Based on this reconstruction, several important beam parameters, including measures of the peak power density and beam width, are determined.

Using this unique diagnostic tool, the effects of changes in the focus setting at constant voltage and current settings on the resulting electron beam parameters have been studied on machines in the U.S. Department of Energy (DOE) complex. Based on these results, the "sharp focus" condition for each welder is determined and given a quantitative definition. Welds are then made on each welder at the machine sharp focus and at a lower peak power density measured using this diagnostic tool in order to compare the response of the welders and to determine the relationship between well characterized beams and the resulting welds. In addition to examining the effects of changes in focus settings, the effects of changes in work distance are also evaluated and used to estimate the lens to workpiece distance. These tests represent a first attempt at the development of a modern electron beam welding transfer procedure.

Experimental

LLNL EB Profiling System

The LLNL EB Profiler system consists of two primary components: a Modified Faraday Cup (MFC) to capture the beam in the welding chamber and a software package for data acquisition and reconstruction of the beam. A photograph of the present version of the Modified Faraday Cup and a schematic illustration of the basic components of the device are shown in Figures 1(a&b), respectively. In the schematic drawing in Figure 1(b), the primary components in the MFC device are identified and are described in more detail elsewhere.[9]

In this design, a number of enhancements have been incorporated to improve both the performance of the device as well as to improve the quality of the data captured using it. Electron capture is enhanced in this design through an additional slit disk, made of copper, which is placed at the top of the internal Faraday cup. This copper slit disk captures the majority of the backscattered electrons and prevents them from leaving the Faraday cup. A beam trap is placed inside of the MFC to provide even more containment of the electron beam when the full beam current is being measured through the center hole of the MFC. A graphite ring was placed below the copper slit disk, and a graphite disk was added at the bottom of the beam trap to minimize the amount of backscattered electrons that pass through the slits. Electrical grounding of the tungsten slit disk is insured using a 0.020 inch diameter tantalum wire was vacuum brazed to the tungsten slit disk and then attached to the copper heat sink body. In addition, a copper clamp

was employed to maintain pressure on the tungsten slit disk and thus maintain good electrical and thermal contact with the heat sink body.

In order to capture the electron beam, the electron beam is captured by the Modified Faraday Cup as it is deflected along a circular path approximately 25.4 mm in diameter. Unlike a traditional Faraday Cup, which contains a single small hole, the Modified Faraday Cup design contains 17 linear slits placed at radial angles around a tungsten slit disk (See Figure 2(a).). When the beam passes over each slit, a portion of the beam current passes into the Faraday Cup and is converted into a voltage drop across a know resistor. This voltage drop is captured by a fast sampling analog-to-digital (A/D) converter, as shown in Figure 2(b). After passing over all 17 radial slits, a waveform containing the 17 resulting peaks is captured by the data acquisition software, as shown in Figure 2(c), and after the application of a digital filtering routine, if necessary, the data are then fed into a computer assisted tomographic (CT) imaging algorithm in order to reconstruct the power density distribution of the beam (See Figure 2(d)).

Once reconstructed, the peak power density of the electron beam and two distribution parameters are determined. The first distribution parameter is the full width of the beam at one-half its peak power density (FWHM). This parameter represents the width at 50% of the beam power. The second parameter, FWe2, is the full width of the beam at $1/e^2$ of its peak power density. This parameter represents the width of the beam at 86.5% of the beam power. Since the cross section of the measured beam is not always circular, the area of the measured beam at these two points is determined, and the diameter of a circle having the same area is used to represent both values. These approximations are good for most beams near sharp focus which generally have cross sectional shapes and have Gaussian like distributions. Figure 2(e) provides an illustration of how these parameters are determined. In Figure 3, a screen snapshot of the data acquisition and reconstruction computer interface is also shown.

Round Robin Testing Between Three Welders

A round robin testing series using the LLNL EB Profiler diagnostic system has been performed on three electron beam welding systems in use within the DOE complex. The general characteristics of these three welders, located at Lawrence Livermore National Laboratory, Los Alamos National Laboratory (LANL), and the BWXT Y-12 Plant, are listed in Table 1. All three welders are capable of accelerating voltages of 150 kV and beam currents of 50 mA. The

LANL and Y-12 machines have build dates within a year of each other and have been produced by the same manufacturer. On the other hand, the LLNL machine, while built by a predecessor to the manufacturer of the other two machines, is of a much older vintage and lacks many of the modern features of the other two machines.

The three welders used in this study are characterized primarily by examining the effects of changes in focus on the beam parameters through a series of defocus runs performed on each machine. In each defocus run, the beam produced at the operator sharp focus is first characterized. Beams produced at focus settings both above and below the operator focus settings are then characterized, thus allowing the focus responses of the three machines to be determined with respect to the peak power density, FWHM value, and FWe2 value. The beam acquisition and computer tomographic parameters used in characterizing the beams are listed in Table 2.

After characterizing each machine, welds are made using the weld conditions described in Table 3. In general, each autogenous weld is made at a constant power of 1 kW and the other essential electron beam welding parameters remain constant. The only variable changing between welds in the round robin study is the focus setting, which is varied from the machine sharp focus to a positive defocus value which produces a beam with a peak power density of 18000 W/mm^2. All welds are made on 304L stainless steel samples, with a thickness of 9.5 mm. These samples are fabricated from material taken from a single heat, and the chemical composition is given in Table 4. After welding, samples are removed from each weld and the resulting weld pool cross sections are metallographically prepared and etched using an electrolytic oxalic acid solution to expose the fusion zones. Depth and width measurements are then made on each cross section, and the results obtained from the different welders are compared.

Results and Discussion

Determination of Sharp Focus, and Measuring Welder Focus Response

The focus response for each welder is characterized by measuring the peak power density at focus settings ranging from approximately 25 mA above to 25 mA below the operator determined sharp focus setting. By measuring the peak power density, the sharp focus setting can be determined for a given set of machine parameters. A typical example of the relationship

between the peak power density and the focus coil current setting is shown in Figure 4(a) for a 100 kV, 10 mA beam produced by the LLNL welder. In this figure, the peak power density curve displays a maximum value at a focus setting of 446 mA and decrease to much lower values at focus settings both above and below this value.

The operator determined sharp focus setting is indicated on the plot at a value of 450 mA. In the absence of modern diagnostic tools, this setting has typically been considered to be the sharp focus setting. This setting should, in turn, correspond to that at which the highest peak power density is observed using the LLNL Beam Profiler. In this case, the two values differ by 4 mA (446 mA vs. 450 mA). Because the highest measured peak power density value is a quantitative measure of the beam properties, as determined by the diagnostic tool, it is used to define the machine sharp focus setting.

The focus coil current settings are converted to machine focus settings using this 4 mA offset. These machine focus settings are then plotted in Figure 4(b) with the corresponding peak power density values. In this plot, the machine sharp focus setting, defined by the focus coil current setting at which the highest peak power density is measured, is set to zero. Focus coil current settings above this value are given a positive value, while those below are given a negative value. Since the focus coil current settings can vary between welders, a relative machine focus setting is more useful when comparing the different welders. This convention for defining the machine focus is used exclusively throughout the remainder of this document.

The peak power density and FWHM and FWe2 values for the three welders at their respective machine sharp focus setting are given in Table 5. A comparison of the reconstructed beams at the machine sharp focus setting of each welder is shown in Figures 5(a-c). The beams produced by the three welders vary both in shape and in the power density distribution across the width of the beam. Of the three welders, the LANL welder displays the highest peak power density and narrowest beam. The Y-12 welder displays the next highest peak power density, and the LLNL welder displays the lowest value.

Comparisons of the results taken over the full range of the defocus runs performed on the three welders are shown in Figures 6(a-c). In these figures, the peak power density, FWHM, and FWe2 values, respectively, are plotted as a function of the machine focus settings. The three welders display similar trends in each figure. For example, the peak power density values are highest at the machine sharp focus setting and rapidly decrease with increasingly positive and

negative defocus settings. On the other hand, FWHM and FWe2 values plotted in Figure 6(b) and 6(c) display minimum values at the machine sharp focus settings and slowly increase in size at higher positive and negative defocus settings. Since the beam width measurements increase rather slowly at small defocus settings, the minimum beam width is not as obvious as the highest peak power density.

The welders also display differences in their response to beam defocusing. Differences are evident in the measured peak power density values, which are plotted as a function of the focus settings for the three welders in Figure 6(a). In Figures 6(b) and 6(c), the FWHM and FWe2 values for the LANL welder display different trends than those observed for the LLNL and Y-12 welders. Whereas the Y-12 and LLNL welders display similar beam widths at specific negative and positive defocus settings, the LANL welder displays a wider beam under positive defocus conditions than at the equivalent negative defocus condition. These differences in the focus response of the three welders illustrate how characteristics of each welder differ, even at nominally the same beam parameters.

Round Robin Welding Study on Stainless Steel

Figures 7(a-c) display the weld cross sections produced by the LLNL, LANL, and Y-12 welders at their respective machine sharp focus settings. The width, depth, aspect ratio, and cross sectional area measurements for each weld, along with the corresponding beam parameters, are included in Table 5. As shown in both Figure 7 and Table 5, the three welders produce significantly different weld cross sections at their respective machine sharp focus conditions.

Of the three welds, the one produced by the LANL welder, which exhibits the highest peak power density, is the deepest and narrowest. The welds produced by the LLNL and the Y-12 welders display smaller depths and larger widths, which are consistent with the lower peak power density values and larger beam widths measured at the machine sharp focus setting for these two welders. These results show that the machine sharp focus condition in different welders can produce welds with different dimensions, even though all other welding parameters are held constant. Therefore, another measure of describing the beam properties must be used in order to effectively transfer beam parameters between different machines.

In order to compensate for the different characteristics of the three machines and to produce similar welds on each machine, welds are produced at a constant peak power density value. The

peak power density is used because, unlike the beam width measurements, the peak power density exhibits an easily identifiable peak value and measurable differences at the lower defocus settings (See Figure 6(a)). The sensitivity of this parameter to small changes in the focus setting make it an attractive means for defining electron beams to be used in welding.

Since the three welders display different defocus responses, different focus settings are required to attain a constant peak power density value of 18000 W/mm^2. As shown in Table 5, the LLNL welder displays the smallest defocus value (+3) and the LANL welder displays the highest defocus value (+7), both of which are consistent with the differences in the peak power density values measured at the machine sharp focus settings. The resulting peak power density values display a variation of at most 5% from the target value, with the most significant deviation from being displayed by the Y-12 welder. Both the FWHM and FWe2 values for each welder are similar in magnitude as well, although the Y-12 welder consistently displays the highest width values.

Figures 8(a-c) show the resulting weld cross sections made at the positive defocus settings required to produce a peak power density value of 18000 W/mm^2 on each welder. Table 5 also summarizes the weld dimensions measured for each weld. As expected, these welds are shallower and wider than those produced at the machine sharp focus settings. Of greater interest, though, is the comparison between the weld dimensions and shapes produced by the three welders at nominally the same peak power density value.

There are a number of similarities and differences between the three welds. The welds produced by the LLNL and LANL welders display very similar depths, but the width of the LANL welder measured at the sample surface is upwards of 25% higher than that produced by the LLNL welder. The Y-12 welder produces a weld with a depth approximately 15% lower and a width nearly 40% greater than the LLNL welder. Whereas the Y-12 welder has the lowest peak power density value of the three welders, albeit by only a value approaching 5%, such a large difference in the weld depth is not expected.

These differences in the welds produced at nominally the same peak power density values indicate that there are other differences in the beams produced by each welder. In order to better understand these differences, a closer examination of the beams used to produce these welds is required. Figures 9(a-c) show the reconstructed power density distributions for the beam used to produce each weld. Differences in the shapes of the beams are evident. For example, the beam

produced by the LANL welder (Figure 9(b)) is elongated along a single axis, making it much more elliptical than the beams produced by the other three welders. The beams produced by the LLNL and Y-12 welders at lower defocus settings are less elongated and more circular. These differences are, in part, expected because of the differences in focus settings required to produce the same peak power density from each welder.

Effect of Work Distance on Electron Beam Properties

Like the changes in focus settings described in the previous section, variations in the work distance also affect the beam properties. It is known, at least qualitatively, that changes in the work distance vary the beam spot size as well as the power density. A quantitative measure of the effects of changing work distance and focus setting on the resulting beam characteristics is undertaken using the LLNL Beam Profiler. The effects of changes in the work distance from 127 mm to 457 mm, as measured from the top of the chamber, on the peak power density, FWHM, and FWe2 values at a range of focus settings on the LLNL welder are plotted in Figures 10(a-c), respectively. A summary of the beam parameters measured at the machine sharp focus condition for each work distance is also given in Table 6.

Changes in work distance have a significant impact on the peak power density and peak width measurements across the range of focus settings. At shorter work distances, the beams display much higher peak power densities and narrower beams than those produced at the longer work distances. The observed trends in the beam parameter values with changes in the relative focus settings are also affected by changes in work distance. For example, the peak power density measurements at shorter work distances rapidly decrease as the focus settings move above or below the machine sharp focus, resulting in a sharply defined peak power density. With increasing work distance, the slopes of the curves representing the beam parameters decrease in the vicinity of the machine sharp focus setting and display a more flattened appearance.

Since changes in work distance have such a pronounced impact on the beam parameter measurements, a similar response is expected on the resulting weld dimensions. Figures 11(a-e) show micrographs of the weld pool cross sections corresponding to the five work distances discussed above. A summary of the weld pool dimensions is also given in Table 6. As with the beam parameters, the changes in work distance have a significant impact on the resulting weld

pool cross sections. For example, at the shorter work distances, the resulting welds are deep and narrow, as displayed in Figure 11(a) at a work distance of 178 mm. As the work distance increases, the welds become shallower and wider. These changes in weld dimensions are consistent with the changes observed in the beam parameters.

The effects of changes in work distance on the measured beam parameters have also been investigated on the LANL welder. A summary of the beam parameters at the machine sharp focus settings is given in Table 7. The response of the different parameters to changes in work distance is similar to that of the LLNL welder. For example, the peak power density measured at the machine sharp focus setting decreases, while the FWHM and FWe2 values increase, with increasing work distance.

Experimental Determination of the Location of the Focusing Lens

The welds described in the round robin testing section are made at nominally the same voltage, current, chamber pressure, travel speed, and work distance. Differences which have arisen in the beams produced by the different welders indicate that there are other factors which may contribute to the differences observed in the resulting weld pool cross sections. In particular, the work distance used in these experiments is measured from the top of the chamber to the surface of the work piece. Even though this method of measuring the work distance provides a means of consistently obtaining the same work distance, it does not take into account differences in the location of the electron focusing lens in the upper column of each electron beam welder.

The electron focusing lens is capable of focusing the beam over a range of work distances within the chamber. Changes in the focal length of the beam affect the diameter of the beam at its sharpest focus (cross-over) condition. At shorter work distances, the minimum beam diameter decreases, resulting in a more intense beam than can be produced at longer work distances. Changes in the divergence angle also occur as the focal length of the beam is changed. As the work distance decreases, the focal length of the lens decreases and the beam divergence angle increases. This results in a condition in which only small changes in the focus setting near the machine sharp focus condition produce large changes in the peak power density and beam width.

The measured variations in beam properties as a function of work distance were shown in Figure 10 for a range of work distances from 127 to 457 mm on the LLNL welder. This information would be more useful if it could be expressed as a function of focal length of the electron lens instead of working distance in the welder, since the focal length of the lens is a parameter that can be transferred from one machine to another. Using the FWHM and FWe2 information provided in Fig. 10, the location of the focusing lens and, in turn, the lens-to-work piece distance can be determined. To do this, the FWHM and FWe2 values for the LLNL welder are first plotted as a function of the work distance in Figure 13a. Both parameters display a linear trend and can be extrapolated back to their work-distance axis intercepts. This intercept location approximately marks the point where the focusing lens is located, since the FWHM and FWe2 would be expected to approach values near zero as the focal length approaches zero at the lens location.

The data from Fig 13a were then fit using a linear regression analysis, and the equations representing the results from these analyses are also shown on the plot. The FWe2 and FWHM values measured on the LLNL welder display similar slopes and intersect the work distance axis at similar locations, 156 mm and 136 mm respectively, above the top of the vacuum chamber wall of the electron beam welder. Thus, from this information, the focal length of the electron beam can be determined by adding this distance to the work distance measured inside the electron beam chamber. The FWHM and FWe2 estimations of the lens location differ slightly due to imperfect optics that lead to non-ideal beams, and also due to scatter in the experimental data. Additional experiments are planned at different kV and mA beam settings to determine how accurately this method can determine the lens location.

The data presented in Fig. 13a provide a convenient method for selecting a given beam size, by choosing the work distance accordingly and the regression equations for FWHM and FWe2. This approach can further be extended to the peak power density. Figure 13b shows this relationship, where the peak power density is plotted as a function of work distance based on the data presented in Figure 10a. In Fig 13b, the five different work distance data points are fit with a curve that predicts the peak power density from the power and measured FWHM of the beam using the following relationship for Gaussian shaped beams:

$$\text{PPD } (W/mm^2) = kV*mA/(2\pi(FWHM/2.35)^2)$$

where FWHM is in mm, kV is the beam voltage, and mA is the beam current. The factor of 2.35 is related to the relationship between the standard deviation of a Gaussian beam and it's FWHM [7]. The predicted data fits the data points very well, and allows the work distance to be set for a desired peak power density for these welding parameters on the LLNL electron beam welder.

To see if the lens-to-part distance can vary between welders, a series of defocus runs were made at different work distances on the LANL welder as well. These data are summarized in Fig 14, which compares the FWe2 values for the LLNL and LANL welders as a function of work distance. The two machines display a difference of approximately 44 mm (156 mm for the LLNL welder and 112 mm for the LANL welder) in the estimated locations for the focusing lenses. Since the location of the focusing lens in the LANL welder is closer to top of their vacuum chamber than for the LLNL welder, the lens-to-part distance of the LANL welder is less than that of the LLNL welder for identical working distances. This means that the LANL welder would be expected to have a more intense beam than the LLNL welder for the experiments performed in this study. This fact is evident when reviewing the data presented in Fig 6, which shows that the LLNL welder has a peak power density approximately 25% less than the LANL and Y-12 welders. This would also explain the difference in weld properties of the sharpest focused beams on each welder, where the LANL welder produced deeper penetration welds than the LLNL welder. Additional experiments are planned on the Y-12 welder to determine its lens location, which is expected to be similar to that of the LANL welder due to the similarities in the beam properties that were measured with the electron beam profiler.

Summary and Conclusions

This study represents the first attempt to characterize multiple welders using an advanced diagnostic tool, and to use this tool to transfer electron beam welding parameters between machines. The use of the LLNL EB Profiler in this capacity has illustrated the differences in the beam characteristics produced by these different machines under nominally the same conditions. Most importantly, the importance of using the lens-to-part distance rather than the conventional work distance parameter to transfer parameters between machines has been demonstrated. The

results from this study are based on the results gathered on three different electron beam welding machines in use within the U.S. DOE complex are as follows:

- The effects of changes in the focus setting at a constant voltage, current, chamber pressure, and work distance on the peak power density and width of the beam have been examined. These defocus studies showed differences in the characteristics of the three machines, even though the general machine settings were maintained constant.
- Using the results from these defocus studies, welds were made on stainless steel samples using each welder at their respective sharp focus settings, and also at a constant peak power density of 18,000 W/mm^2. The welds made at the machine sharp focus condition displayed significant differences in both depth and width, resulting from variations in the beam parameters measured using the diagnostic tool. Welds made with the same peak power density showed less variations.
- The effects of work distance on the beam parameters were investigated in the LLNL and LANL welders for work distances between 127 mm and 584 mm. These work distances were measured from the top of the welding chamber to the top of the work piece, and were shown to have a dramatic influence on the beam. In particular, the peak power density values measured at the longer work distances are much lower than those measured at the shorter work distances. This variation in work distance resulted in caused an approximate 33% decrease in the weld depth when using the sharpest focused beam at each work distance.
- The location of the electron focusing lens in the upper EB weld column was estimated using the beam width measurements made using the LLNL EB Profiler at different work distances. Based on these estimations, the locations of the electron focusing lens of the LLNL welder was nearly 44 mm higher up in the column than the LANL welder. This difference resulted in a hotter, more tightly focused, electron beam on the LANL welder than the LLNL welder, and observed by in the peak power density, FWHM, and FWe2 properties measured on each machine.

Acknowledgments

This document was prepared as an account of work sponsored by an agency of the United States Government. Neither the United States Government nor the University of California nor any of their employees, makes any warranty, express or implied, or assumes any legal liability or responsibility for the accuracy, completeness, or usefulness of any information, apparatus, product, or process disclosed, or represents that its use would not infringe privately owned rights. Reference herein to any specific commercial product, process, or service by trade name, trademark, manufacturer, or otherwise, does not necessarily constitute or imply its endorsement, recommendation, or favoring by the United States Government or the University of California. The views and opinions of authors expressed herein do not necessarily state or reflect those of the United States Government or the University of California, and shall not be used for advertising or product endorsement purposes. The LLNL portion of this work was performed under the auspices of the U.S. Department of Energy by University of California, Lawrence Livermore National Laboratory under Contract W-7405-Eng-48. The LANL portion of this work has been supported by the Los Alamos National Laboratory, which is operated by the University of California for the U.S. Department of Energy under Contract No. W-7405-ENG-36. The Y-12 portion of this work has been supported by the Y-12 National Security Complex, Oak Ridge, TN 37831-8169, managed by BWXT Y-12, L.L.C. for the U.S. Department of Energy under contract DE-AC05-00OR22800.

References

1. Recommended Practices for Electron Beam Welding, 1999, ANSI/AWS C7.1-99, Miami, FL, American Welding Society.
2. G. R. LaFlamme and D. E. Powers: *Welding Journal*, 1991, **70**(10): pp. 33-40.
3. U. Dilthey and J. Weiser: *Schw. and Schn.*, 1995, **47**(7): pp. 558-564.
4. U. Dilthey and J. Weiser: *Schw. and Schn.*, 1995, **47**(5): pp. 339-345.
5. J. W. Elmer and A. T. Teruya, "An Enhanced Faraday Cup for the Rapid Determination of the Power Density Distribution in Electron Beams," *Welding Journal*, 80(12), 288s-295s, 2001.
6. J.W. Elmer and A.T. Teruya, "Fast Method for Measuring Power Density Distribution of Non-Circular and Irregular Electron Beams," *Science and Technology of Welding and Joining*, 3(2), 51-58, 1998.

7. J.W. Elmer, A.T. Teruya, and D.W. O'Brien, "Tomographic Imaging of Noncircular and Irregular Electron Beam Current Density Distributions," *Welding Journal*, 72(11), 493s-505s, 1993.

8. A. Teruya, J. Elmer, and D. O'Brien, "A System for the Tomographic Determination of the Power Distribution in Electron Beams," in The Laser and Electron Beam in Welding, Cutting, and Surface Treatment: State-of-the-Art 1991, Bakish Materials Corp., Englewood, NJ, 1991, pp. 125-140.

9. J.W. Elmer, A.T. Teruya, and T.A. Palmer, "User's Guide: An Enhanced Modified Faraday Cup for the Profiling of the Power Density Distribution in Electron Beams", Lawrence Livermore National Laboratory Document UCRL-MA-148830, 2002.

Table 1. Characteristics of electron beam welders used in this study.

	Welder #1	**Welder #2**	**Welder #3**
Location	Lawrence Livermore National Laboratory	Los Alamos National Laboratory	BWXT Y-12 Plant
Manufacturer	Hamilton Standard	Leybold Herareus	Leybold Herareus
Serial number	175	663	649
Voltage (kV)	150	150	150
Current (mA)	50	50	50
Filament Type	Ribbon	Ribbon	Ribbon
Electron Gun Type	R-40	CL-R167-R	R167-R
Year of Manufacture	1965	1985	1984

Table 2. Summary of data acquisition input parameters used in the EB Profiler software.

Data Acquisition Parameters	**Values**
Scan Rate (Scans/sec)	250000
Beam Deflection Frequency (Hz)	30
Deflection Direction	CCW
Profile Length	490
Resize Factor	1
Sinogram Filter	None

Table 3. Summary of electron beam welding parameters used in the round robin study.

Essential Electron Beam Parameters	**Test #1**	**Test #2**
Voltage (kV)	100	100
Current (mA)	10	10
Relative Work Distance[a] (mm)	229	229
Chamber Pressure (Pa)	0.0067	0.0067
Travel Speed (mm/sec)	17	17
Focus Condition	Sharp	18 kW/mm^2 [b]

[a] Work distance is measured from the top of the weld chamber to the top surface of the part.
[b] Welds are made at a constant measured peak power density.

Table 4. Chemical composition of 304L stainless steel samples used in the round robin welding study. All values are in wt.%.

Fe	**Cr**	**Ni**	**Mn**	**Mo**	**C**	**N**	**Si**	**Co**	**Cu**	**S**	**P**
Bal.	18.20	8.16	1.71	0.47	0.020	0.082	0.44	0.14	0.35	0.0004	0.03

Table 5. Summary of electron beam characteristics measured in each welder during the round robin tests.

	LLNL Welder		LANL Welder		Y-12 Welder	
	Task #1	**Task #2**	**Task #1**	**Task #2**	**Task #1**	**Task #2**
Focus Coil Current (mA)	446/MS[a]	449/+3	650/MS[a]	657/+7	679/MS[a]	684/+5
Peak Power Density (W/mm^2)	19997	17490	28093	18426	24621	17073
FWHM (mm)	0.210	0.220	0.163	0.204	0.190	0.224
FWe2 (mm)	0.346	0.365	0.290	0.354	0.311	0.379
Weld Depth (mm)	3.97	3.82	4.86	3.91	3.81	3.23
Weld Width (mm)	1.49	1.52	1.38	1.91	1.72	2.14
Aspect Ratio	2.67	2.51	3.52	2.05	2.22	1.51
Cross Sectional Area (mm^2)	2.63	2.66	2.47	2.76	2.22	2.20

[a] MS = Machine sharp focus

Table 6. Summary of beam parameters made at the machine sharp focus setting measured at each work distance on the LLNL welder.

	Work Distance (LLNL Welder, H.S. Ser # 175)				
	127 mm	***229 mm***	***305 mm***	***381 mm***	***457 mm***
Peak Power Density (W/mm^2)	34894	19997	14111	10160	7791
FWHM (mm)	0.155	0.210	0.251	0.298	0.344
FWe2 (mm)	0.262	0.346	0.413	0.486	0.557
Weld Depth (mm)	4.46	3.97	3.69	3.39	2.96
Weld Width (mm)	1.27	1.48	1.48	1.55	1.71
Aspect Ratio	3.52	2.65	2.49	2.19	1.73
Cross Sectional Area (mm^2)	2.40	2.63	2.58	2.56	2.62

Table 7. Summary of beam parameters made at the machine sharp focus setting measured at each relative work distance using the LANL welder.

	Work Distance (LANL Welder, L.H. # 663)				
	178 mm	***254 mm***	***330 mm***	***508 mm***	***584 mm***
Peak Power Density (W/mm^2)	44084	34261	23276	12267	9328
FWHM (mm)	0.134	0.147	0.191	0.242	0.273
FWe2 (mm)	0.230	0.267	0.311	0.463	0.520

(a)

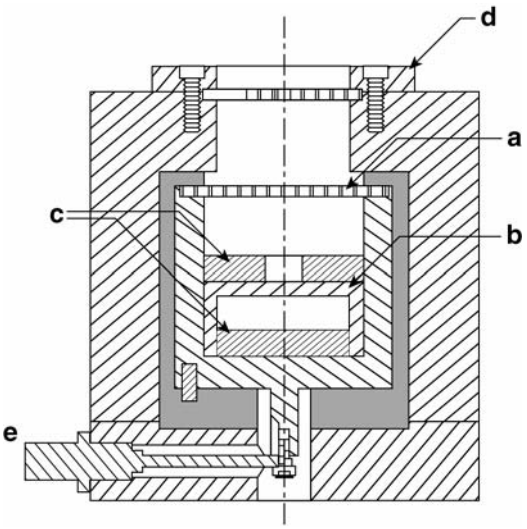

(b)

Figure 1(a&b). (a) Photograph of the enhanced Modified Faraday Cup and (b) a schematic cross sectional illustration of the enhanced MFC diagnostic with the following components identified: a. an internal slit disk made of copper, b. an internal beam trap, c.graphite beam interceptors, d. a clamp for the tungsten slit disk, and e. an integral BNC connector.

(a)

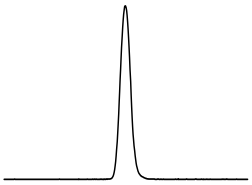

(b)

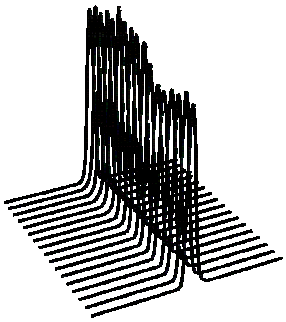

(c)

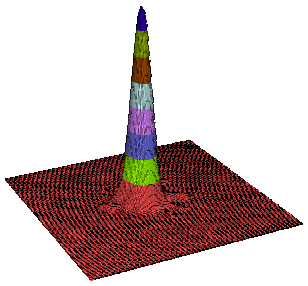

(d)

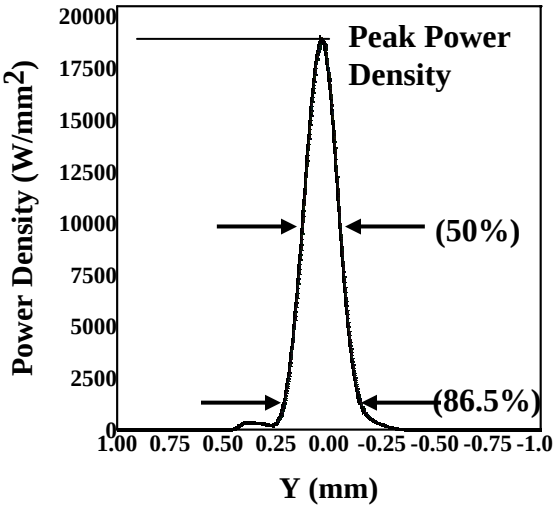

(e)

Figure 2(a-e). Basic overview of operation of the LLNL EB Profiler system beginning with (a) capture of the beam by a 17 slit tungsten disk, (b) a typical profile acquire through one of the slits, (c) a computed sonogram compiling the profiles seen by all 17 slits, (d) a 3D tomographic reconstruction of the power density distribution of the beam, and (e) a slice through the center of of the beam..

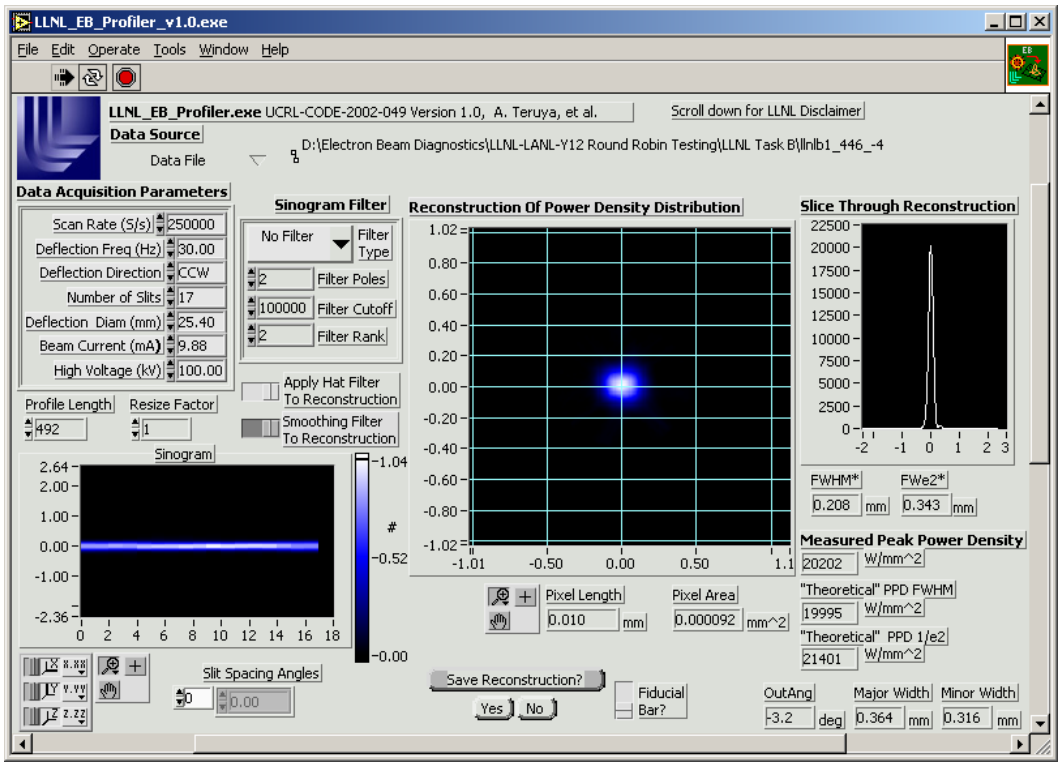

Figure 3. A screen image of the data acquisition and reconstruction software components of the LLNL EB Profiler system.

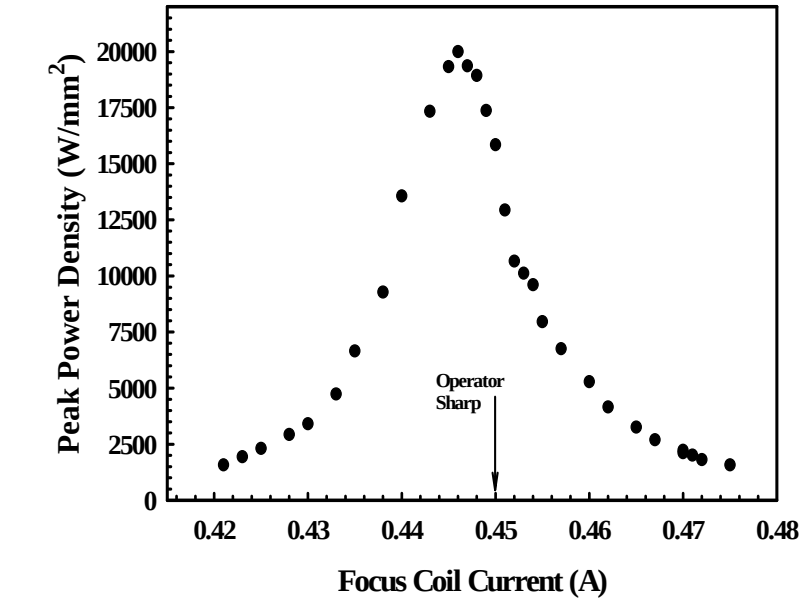

(a)

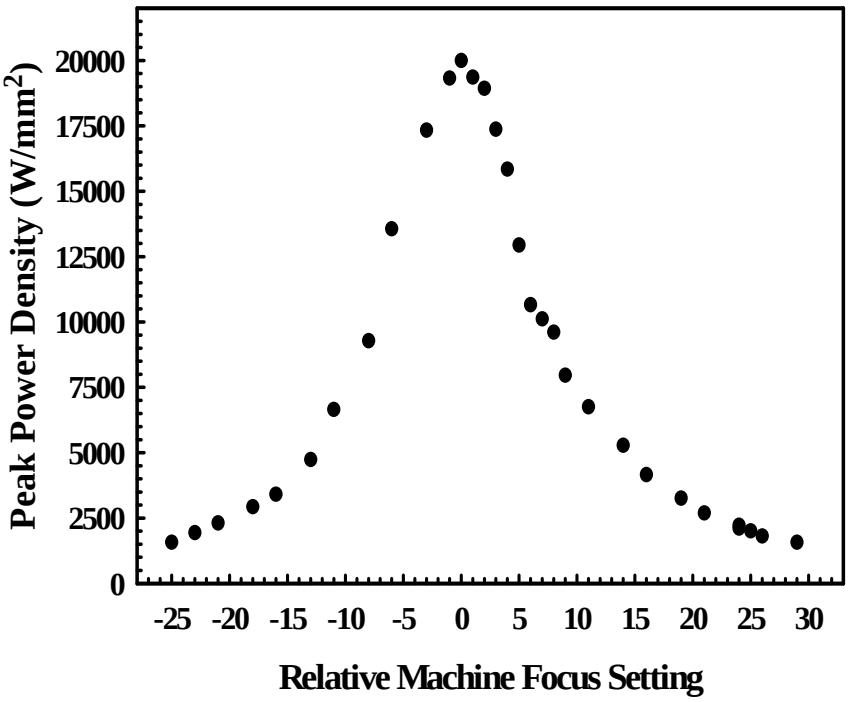

(b)

Figure 4(a&b). (a) Peak power density plotted as a function of the focus coil current for the defocus run made on the LLNL welder, showing the operator determined sharp focus. (b) The same data plotted as a function of the relative machine focus setting.

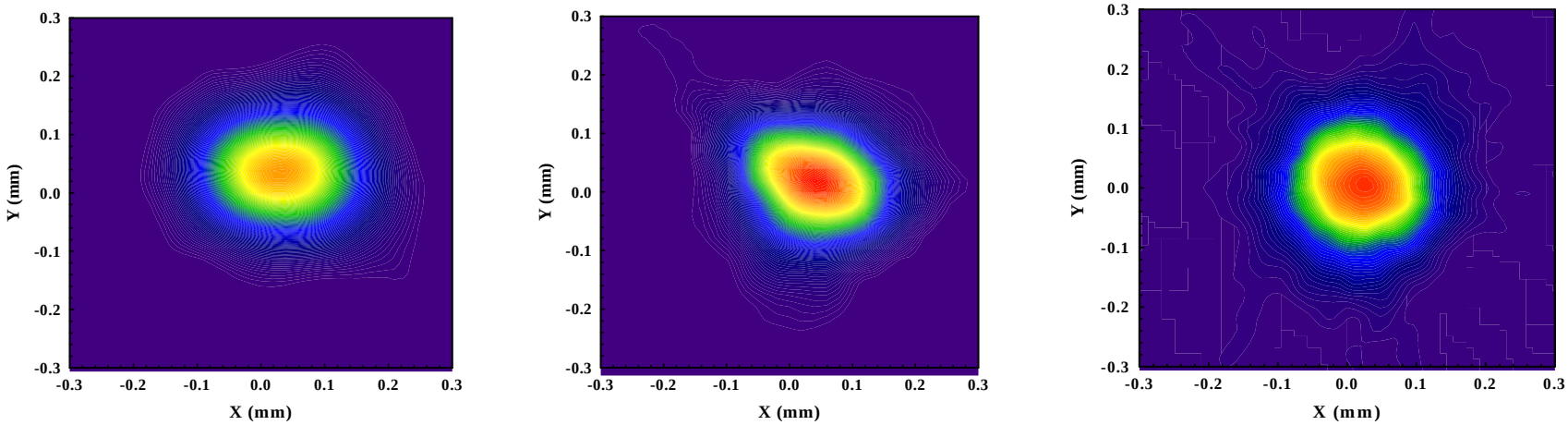

(a) (b) (c)

Figure 5(a-c). Plots comparing the reconstructed beams produced at the machine sharp focus settings for the (a) LLNL welder, (b) LANL welder, and (c) Y-12 welder.

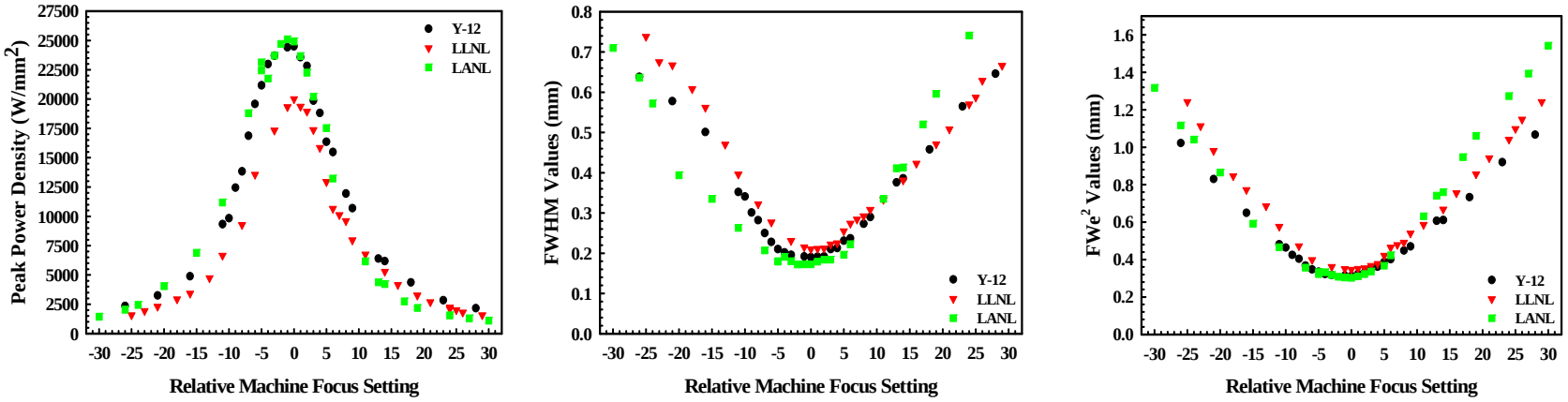

Figure 6(a-c). Plots comparing the measured (a) peak power density, (b) FWHM values, and (c) FWe^2 values with changes in the focus setting on the welders used in the round robin study. All measurements are made using the LLNL EB Profiler.

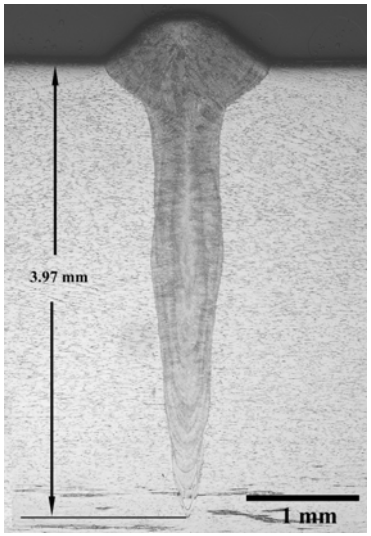

(a)

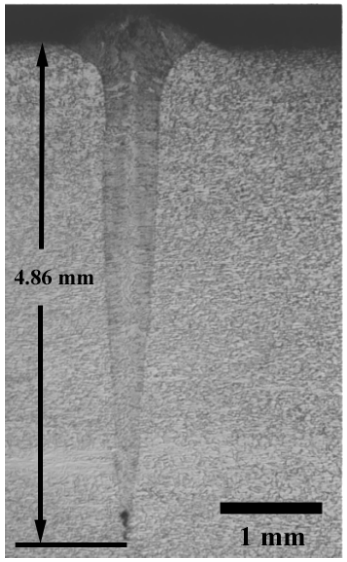

(b)

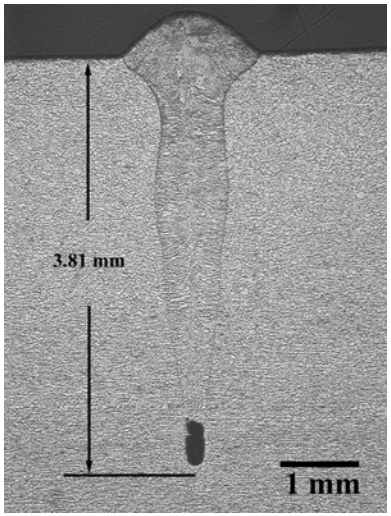

(c)

Figure 7(a-c). Weld cross sections produced in 304L stainless steel samples at the machine sharp focus setting for the (a) LLNL welder, (b) LANL welder, and (c) Y-12 welder.

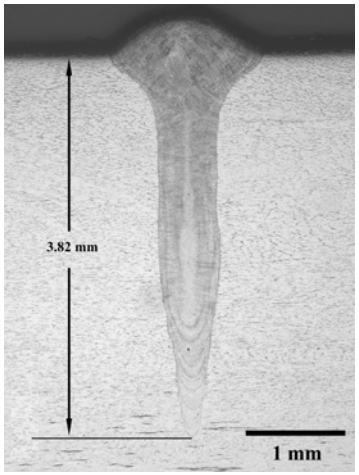

(a)

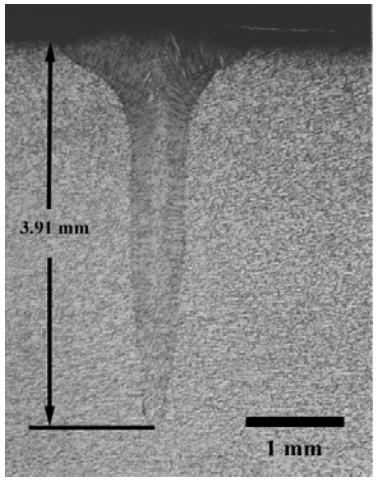

(b)

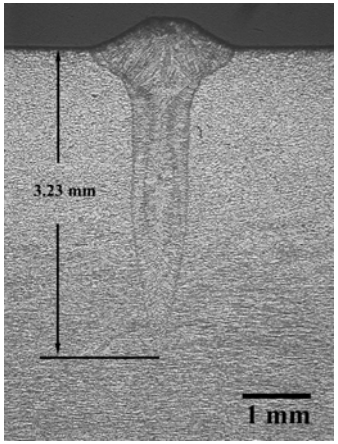

(c)

Figure 8(a-c). Weld cross sections produced in 304L stainless steel samples at focus settings where a peak power density of approximately 18000 W/mm^2 is generated in the (a) LLNL welder, (b) LANL welder, and (c) Y-12 welder.

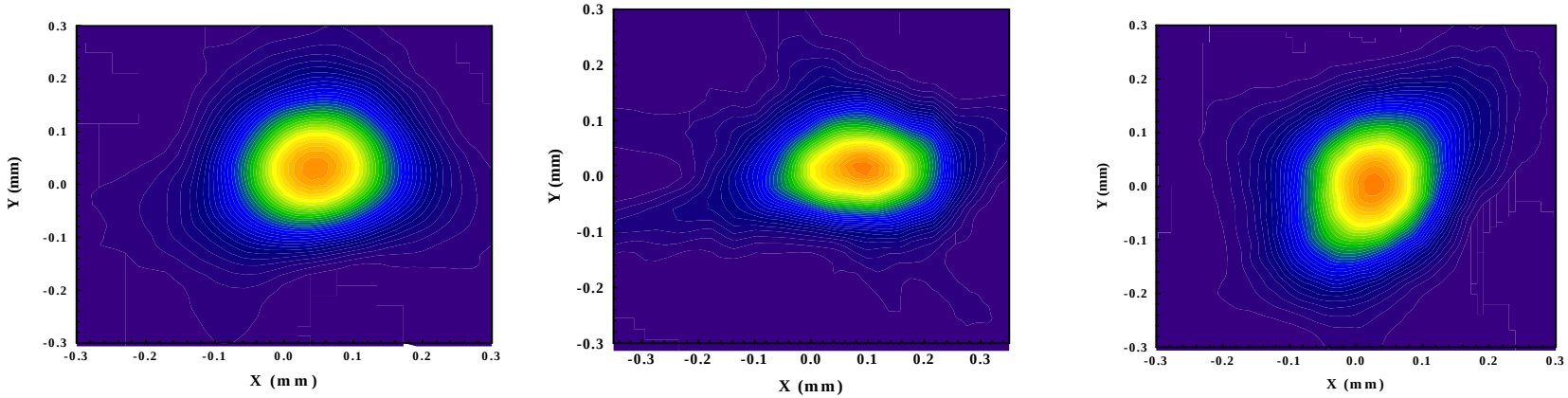

(a) (b) (c)

Figure 9(a-c). Plots comparing the reconstructed beams used to produce the welds made at a constant peak power density of approximately 18000 W/mm^2 in the (a) LLNL welder, (b) LANL welder, and (c) Y-12 welder.

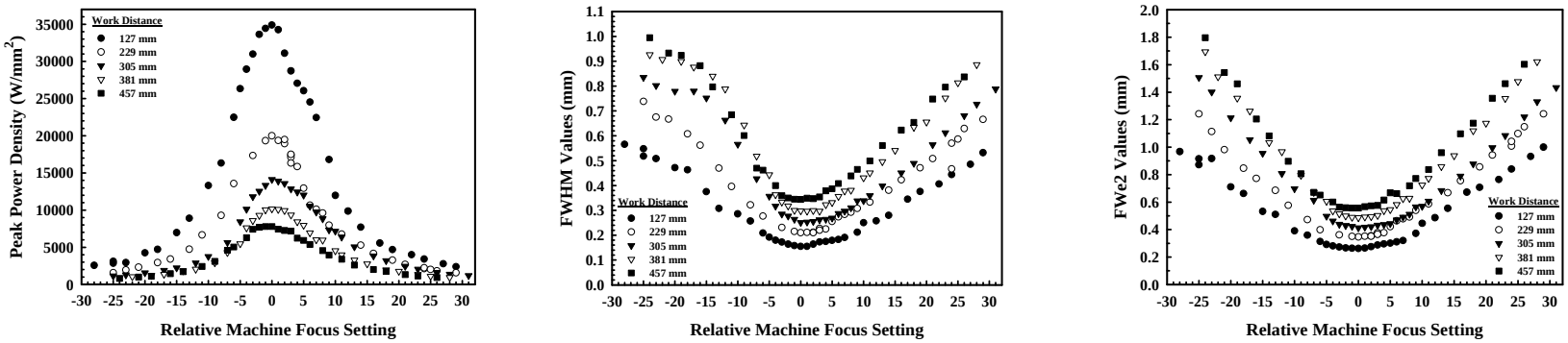

Figure 10(a-c). Plots comparing the measured (a) peak power density, (b) FWHM values, and (c) FWe^2 values with changes in the focus setting at several different work distances on the LLNL welder. All measurements are made using the LLNL EB Profiler.

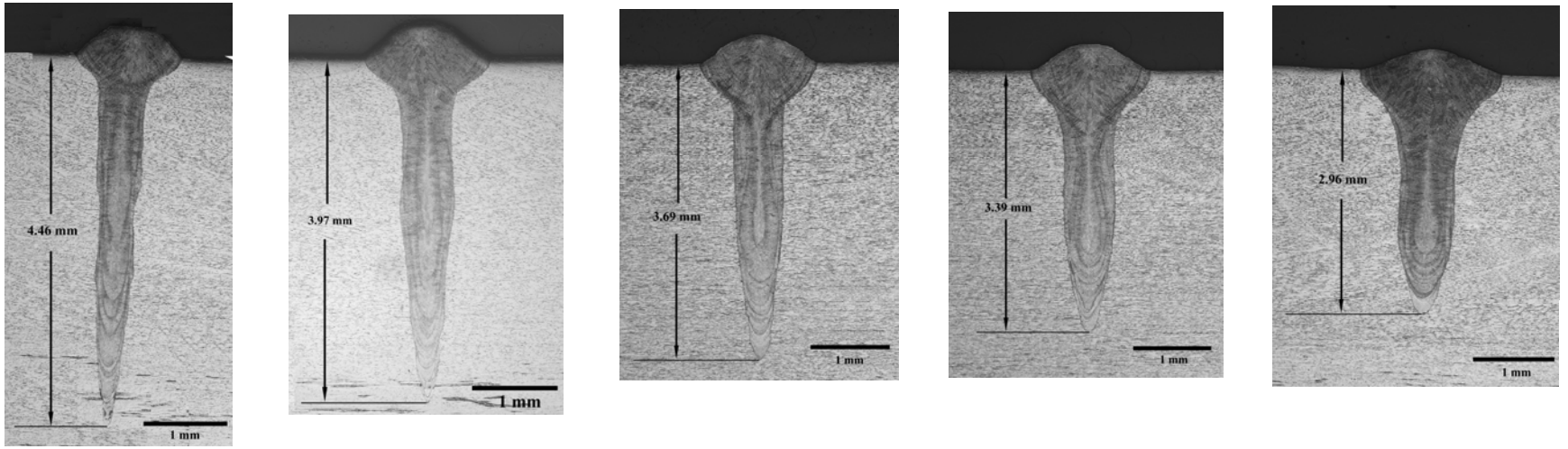

(a) (b) (c) (d) (e)

Figure 11(a-e). Micrographs showing cross sections from welds made at machine sharp focus settings at work distances of (a) 127 mm, (b) 229 mm, (c) 305 mm, (d) 381 mm, and (d) 457 mm.

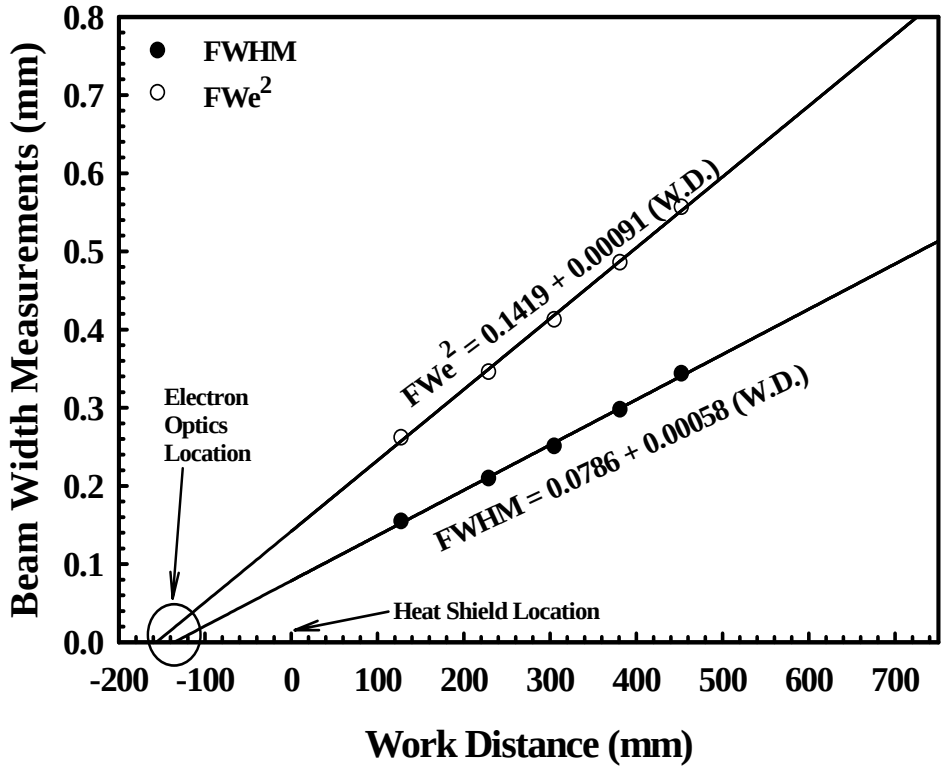

(a)

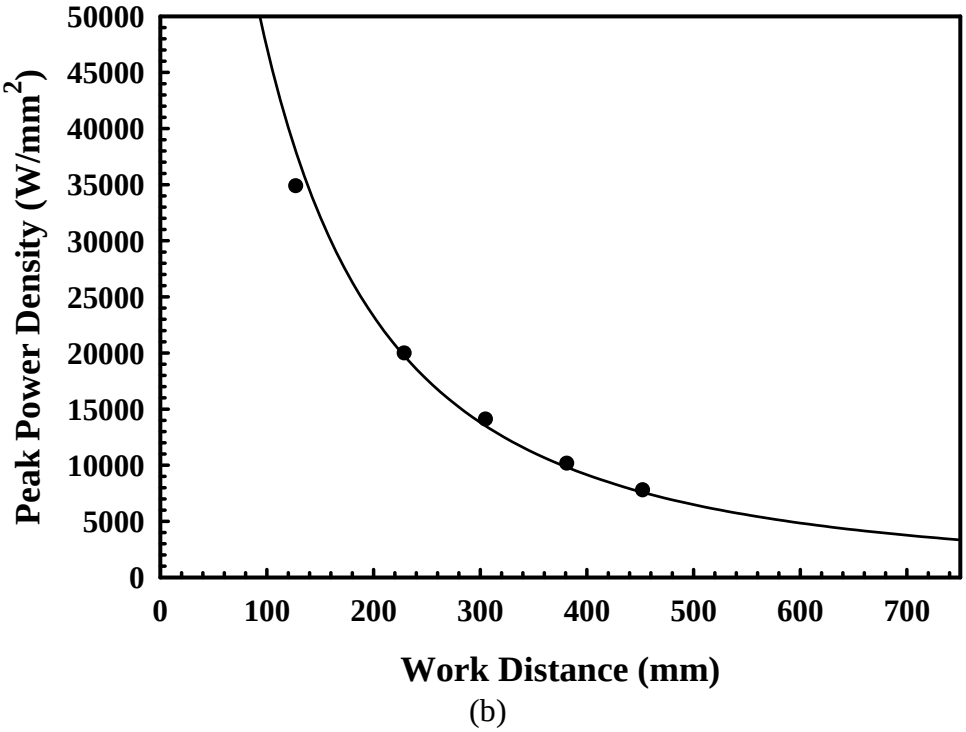

(b)

Figure 13(a&b). Plots showing (a) the relationship between the work distance and the FWHM and FWe2 values and (b) the relationship between the peak power density and the work distance measured on the LLNL welder.

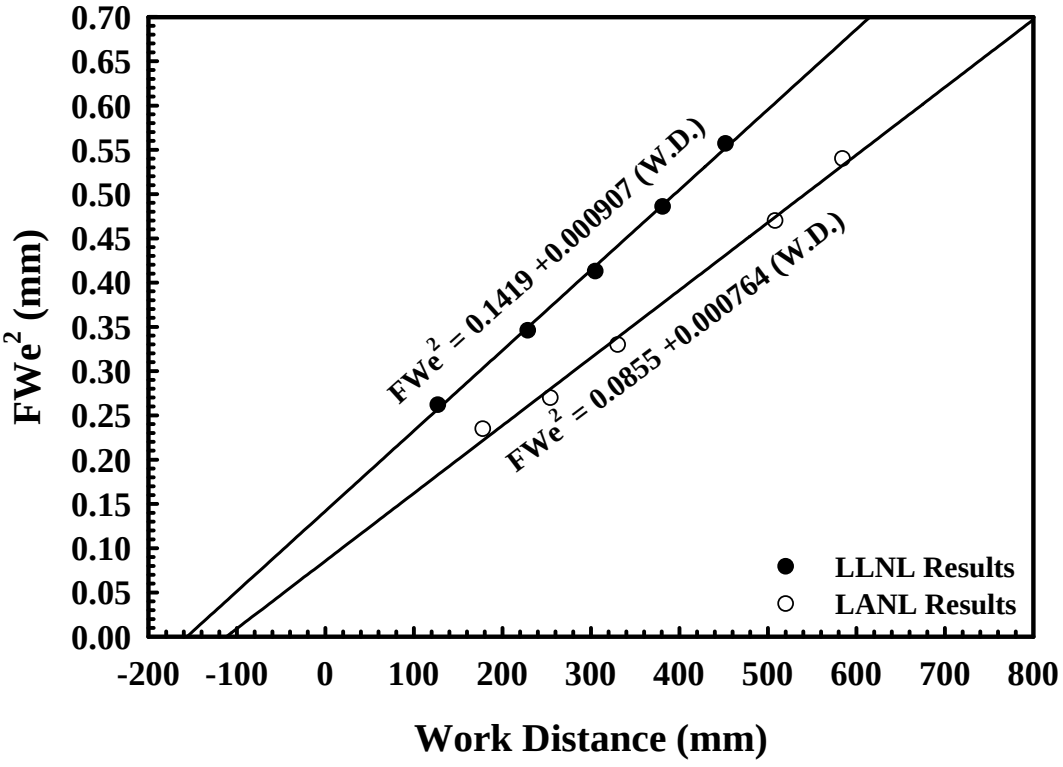

Figure 14. Plot showing comparison between the effects of work distance on the FWe2 values for the LLNL and LANL welders.